Journal of Statistical Physics, Vol. 81, Nos. 1/2, 1995

Scalings in Diffusion-Driven Reaction $A + B \rightarrow C$: Numerical Simulations by Lattice BGK Models

Y. H. Qian[1] and S. A. Orszag[2]

Received November 15, 1994; final May 30, 1995

We are interested in applying lattice BGK models to the diffusion-driven reactive system $A + B \rightarrow C$, which was investigated by Gálfi and Rácz with an asymptotic analysis and by Chopard and Droz with a cellular automaton model. The lattice BGK model is free from noise and flexible for various applications. We derive the general reaction–diffusion equations for the lattice BGK models under the assumption of local diffusive equilibrium. Two fourth-order terms are derived and verified by numerical simulations. The motivation of this study is to compare the lattice BGK results with existing results before we apply the models to more complicated systems. The scalings concern two exponents α and β appearing in the production rate of C component $R(x, t) \sim t^{-\beta} G(xt^{-\alpha})$. We find the same values for $\alpha = 1/6$ and $\beta = 2/3$ as Gálfi and Rácz found at the long time limit. A *Gaussian*-like function for G is numerically obtained, which confirms a similar result of Gálfi and Rácz. On the one hand, when compared with the asymptotic analysis, lattice BGK models are easy to apply to cases where no analytic or asymptotic results exist; on the other hand, when compared with cellular automaton models, lattice BGK models are faster, simpler, and more accurate. The discrepancy of the results between the cellular automaton model and the lattice BGK models for the exponents comes from the role of the intrinsic fluctuation. Once the time and space correlation of stochastic stirring is given, we can incorporate a random fluctuating term in lattice BGK models. The Schlögl model is also tested, showing the ability of lattice BGK models for generating Turing patterns, which may stimulate further interesting investigations.

KEY WORDS: Reaction–diffusion; BGK model; kinetic theory, numerical simulation.

[1] Department of Applied Physics, Columbia University, New York, New York 10027.
[2] Fluid Dynamics Research Center, Forrestal Campur, Princeton University, Princeton, New Jersey 08544.

822/81/1-2-16

0022-4715/95/1000-0237$07.50/0 © 1995 Plenum Publishing Corporation

1. INTRODUCTION

Reaction–diffusion equations appear in many chemical, biological, and physical systems.[25] They usually involve complicated nonlinear reactions. When driven far from equilibria, the systems show interesting behaviors, such as bistability, temporal oscillations, chemical waves, and phase turbulence. A full molecular description of such systems is difficult because of the wide range of relevant scales in space and time and a direct simulation requires a huge number of particles, which is beyond the ability of the most powerful supercomputers. However, simple alternative models which preserve several features of the full systems and which are easier to simulate on computers can be constructed in a systematic way. One such alternative, the lattice BGK approach, will be presented in this paper. The purposes of this paper are threefold: (1) the first is to check high-order effects for dispersion relations of systems simulated by lattice BGK models; (2) the second is to compare and verify some existing asymptotic results at long times for a specific problem, diffusion-driven reaction, and to show the scaling results of all times (short times and long times); (3) the last is to stimulate further interesting studies by showing the capability of lattice BGK models to generate pattern formations. The paper will be organized as follows: In Section 2 we will specify the front dynamics of $A+B\rightarrow C$ and the Schlögl model. We outline the lattice BGK models for the reactions–diffusion systems in Section 3; numerical results are presented in Section 4. The conclusion is given in Section 5.

2. REACTION–DIFFUSION SYSTEMS

Reaction–diffusion systems can be formulated mathematically as

$$\partial_t \rho_s = \kappa_s \partial_{\alpha\alpha} \rho_s + F_s(\rho) \tag{1}$$

where ρ_s is the density of the sth component, F_s is the reaction function resulting from very complicated chemical reaction processes, and κ_s is the diffusivity. The diffusion effect stabilizes the system, while the reaction may drive the system away from some fixed states. The competition between diffusion and reaction leads to the emergence of spatial or temporal structures at a characteristic scale which depends only on the diffusivities and the eigenvalue of the linearized matrix of the reaction functions around fixed points; the interested reader is referred to a review paper by Koch and Meinhardt.[21]

The Schlögl model[32] describes a single-component auto catalytic system, characterized by

$$F(\rho) = -k_3\rho^3 + k_2\rho^2 - k_1\rho + k_0 \tag{2}$$

where k_i $(i=0, 1, 2, 3)$ are constants. A bistable regime can be reached if these constants are properly chosen. The diffusion–driven reactive system $A+B \rightarrow C$ is an irreversible reaction: the densities of A and B decrease at all times. The reaction function is the same for A and B: $F_a = F_b = -K\rho_a\rho_b$ with K being the reaction rate. The equation for component A is

$$\partial_t \rho_a = \kappa_a \partial_{\alpha\alpha} \rho_a - K\rho_a\rho_b \tag{3}$$

and a similar equation can be written for component B. We specify the following conditions: at $t=0$, one half-space is filled with component A of density ρ_{a0} and the other half with B of density ρ_{b0}; at $x=1$ and $x=L$, $\partial_x \rho_a = \partial_x \rho_b = 0$ for $t>0$.

3. 1D, 2D, AND 3D MODELS

Lattice gas cellular automata (LGCA) models[11, 10] were proposed for simulating the two- and three-dimensional hydrodynamic equations. Compared to traditional methods in computational fluid dynamics (CFD), these models are simple and easy to implement on computers. A variety of applications and generalizations of LGCA have been studied.[9] Concerning reaction–diffusion systems, the Schlögl model,[7] the Maginu model,[23, 6] and the Sel'kov model[33, 19, 15] have been investigated recently by using LGCA models. As an alternative to the macroscopic description of real systems, though LGCA models have many interesting features, they suffer from some intrinsic weaknesses: (1) The construction of the collision matrix associated with a given reaction system is very tedious[20] and the derivation of transport coefficients is very difficult; (2) a high level of statistical fluctuation (which is useful in studying the divergence of transport coefficients[18, 8] when the space dimension D is less than 3) requires the use of a coarse–grain averaging over space or time. The advantages and disadvantages of LGCA have been well understood.[9, 28] The lattice Boltzmann equation (LBE) was introduced to remove some of the drawbacks while keeping the advantages of LGCA models.[24, 17, 1] A further simplification using the BGK procedure[2] was recently studied[30, 4, 31] and applied to the Sel'kov model[27] in two dimensions as an example.

3.1. Pure Diffusion Equation

In lattice BGK models for pure diffusion problems, the propagation step is the same as lattice gas models, while the collision step is just a redistribution of mass in all possible directions. The only quantity con-

served during the redistribution is the total mass. We start with the following evolution equation:

$$N_i(\mathbf{x}+\mathbf{c}_i, t+1) = N_i(\mathbf{x}, t) + \omega[N_i^e\mathbf{x}, t) - N_i(\mathbf{x}, t)] \tag{4}$$

where N_i is the average population of particles with velocity $\mathbf{c}_i$ ($i=1, 2,..., B$) which belongs to a predetermined finite set and ω is the relaxation parameter which satisfies $0 \leqslant \omega \leqslant 2$. The local equilibrium population $N_i^e(\mathbf{x}, t)$ is chosen as

$$N_i^e(\mathbf{x}, t) = t_i \rho(\mathbf{x}, t), \qquad t_i = \frac{1}{B} \tag{5}$$

B is the number of discrete particle velocities. This is a homogeneous equilibrium population in all velocity directions. The macroscopic density, denoted by ρ, is defined by

$$\rho(\mathbf{x}, t) = \sum_i^B N_i(\mathbf{x}, t) = \sum_i^B N_i^e(\mathbf{x}, t) \tag{6}$$

The weighting factor t_i satisfies the normalization constraint $\sum_i^B t_i = 1$. The choice (5) for the equilibrium population, when used together with (4) and (6), will be shown to lead to the diffusion equation. We consider models with the particle velocity set in D dimensions ($D=1$, 2, and 3). The simplest models take the velocity set of $2D$ elements: D directions along the axis and D opposite directions. The rest particles can also be included. Therefore, as explained in ref. 30, the D1Q2 model means the one-dimensional model with two velocities: ($\pm c$); the D2Q4 model is two dimensional and has four directions: ($\pm c$, 0), and (0, $\pm c$). The three-dimensional D3Q6 model has six possible velocity directions: ($\pm c$, 0, 0), (0, $\pm c$, 0), and (0, 0, $\pm c$). This model has the same velocity directions as the Broadwell model in discrete kinetic theory.[13] The equation governing the large-scale dynamics of (4), in which the local equilibrium distribution N_i^e is given by (5), can be derived using a Chapman–Enskog expansion.[3, 10, 28] Since similar procedures for the LGCA and LBE have been used before (see, for example, refs. 9 and 10); here we will only outline the steps necessary to obtain expressions for the transport coefficients. We assume a weak deviation from the local equilibrium $N_i^e(\mathbf{x}, t)$,

$$N_i(\mathbf{x}, t) = N_i^e(\mathbf{x}, t) + \varepsilon N_i^{(1)}(\mathbf{x}, t) + \varepsilon^2 N_i^{(2)}(\mathbf{x}, t) + \cdots \tag{7}$$

where ε is the appropriate Knudsen number. The space and time

derivatives are expressed in terms of multiple-scale variables up to the fourth order in time,

$$\partial_\alpha = \varepsilon \partial_\alpha \tag{8}$$

$$\partial_t = \varepsilon \partial_{t_1} + \varepsilon^2 \partial_{t_2} + \varepsilon^3 \partial_{t_3} + \varepsilon^4 \partial_{t_4} \tag{9}$$

Here the multiple time scales t_1, t_2, t_3, and t_4 should not be confused with the prefactor weighting t_i in the equilibrium. When the total mass is conserved, it follows from (4)–(7) that

$$\sum_i N_i^{(j)} = 0, \qquad j > 0 \tag{10}$$

Using the classic Chapman–Enskog[3] expansion and taking into account the discreteness of the lattice model, we obtain the first-order equation in ε,

$$\partial_{t_1} \rho = 0 \tag{11}$$

and the first-order correction,

$$N_i^{(1)} = -\frac{t_i}{\omega} c_{i\alpha} \partial_\alpha \rho \tag{12}$$

The second-order equation is

$$\partial_{t_2} \rho + \left(1 - \frac{\omega}{2}\right) \partial_\beta \sum_i (c_{i\beta} N_i^{(1)}) = 0 \tag{13}$$

It is easy to check that the condition (10) is satisfied by $N_i^{(1)}$. Substituting (12) into (13), we obtain finally

$$\partial_{t_2} \rho - \frac{c^2}{2D} \left(\frac{2}{\omega} - 1\right) \partial_{\alpha\alpha} \rho = 0 \tag{14}$$

Equations (11) and (14), i.e., the dynamical equations from the two separated time scales $1/\varepsilon$ and $1/\varepsilon^2$, are now reconstituted to obtain the macrodynamical equations for the model. The equation of diffusion equation is obtained from (11) and (14) by multiplying the former by ε and the latter by ε^2 and then adding the two equations. We obtain

$$\partial_t \rho = \kappa_2 \partial_{\alpha\alpha} \rho \tag{15}$$

where the diffusivity κ_2 is given by

$$\kappa_2 = \frac{c^2}{2D}\left(\frac{2}{\omega} - 1\right) \tag{16}$$

We can also obtain higher order equations by carrying the Chapman–Enskog expansion further. This is possible for the diffusion models, while no such equations exist for the lattice gas hydrodynamics.[29] We derive the third-order equation

$$\partial_{t_3}\rho = 0 \tag{17}$$

and the fourth-order equation

$$\partial_{t_4}\rho = -A_1\partial_{\alpha\alpha\beta\beta}\rho - A_2\partial_{\alpha\alpha\alpha\alpha}\rho \tag{18}$$

The coefficients A_1, A_2, and κ_2 in (15) for models including rest particles are obtained after some algebraic calculations,

$$\kappa_2 = \frac{B_m}{B}\frac{c^2}{2D}\left(\frac{2}{\omega} - 1\right) \tag{19}$$

where B_m is the number of nonzero velocities in the model (B is the total number of particle velocities, which is different from B_m if a rest particle is included: $B = B_m + 1$),

$$A_1 = \frac{B_m}{B}\frac{c^2}{2D}\left(\frac{2}{\omega^2} - \frac{2}{\omega} + \frac{1}{4}\right)\kappa_2 \tag{20}$$

$$A_2 = c^2\left(-\frac{1}{\omega^2} + \frac{1}{\omega} - \frac{1}{12}\right)\kappa_2 \tag{21}$$

The final fourth-order equation is

$$\partial_t\rho = \kappa_2\partial_{\alpha\alpha}\rho - A_1\partial_{\alpha\alpha\beta\beta}\rho - A_2\partial_{\alpha\alpha\alpha\alpha}\rho \tag{22}$$

Applying the Fourier transform $\exp(-\Omega t - ikx)$ (k is the wavenumber and Ω the frequency) to the above equation in one-dimensional space, we get the dispersion relation

$$\Omega = \kappa_2 k^2 + (A_1 + A_2)\,k^4, \qquad \kappa_4 = A_1 + A_2 \tag{23}$$

and κ is defined by

$$\kappa = \frac{\Omega}{k^2} \tag{24}$$

After simple algebraic calculations, we find that the critical ω_{cr} across which κ_4 changes sign for different models is given by the following: $\omega_{cr} = 3 - \sqrt{3}$ for D1Q2; $\omega_{cr} = 2$ for D1Q3; $\omega_{cr} = 4\sqrt{3} - 6$ for D2Q5; $\omega_{cr} = 1$ for D3Q6; $\omega_{cr} = 18 - 12\sqrt{2}$ for D3Q7. The D2Q4 model has no such behavior. We will verify these results numerically.

3.2. Reaction Function

The reaction term is treated in a much simpler way than the one used in the LGCA model.[20] The idea is that we can consider the reaction term as a special kind of "forcing" for the diffusion process. We follow the

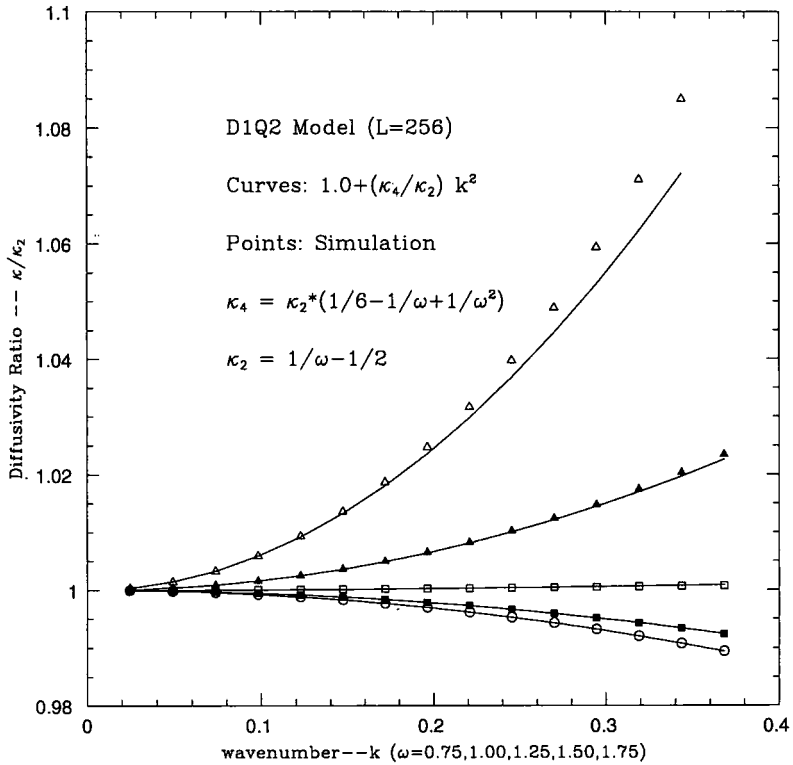

Fig. 1. Dispersion relation κ/κ_2 versus k, with k being the wavenumber. The value of κ/κ_2 decreases as ω increases for the D1Q2 model. The lines are theoretical predictions while the open triangles, solid triangles, open squares, solid squares, and open circles are numerical simulations for $\omega = 0.75$, 1.00, 1.25, 1.50, and 1.75, respectively. The critical ω_{cr} across which the κ_4 changes sign is $\omega_{cr} = 1.26795$ for this model.

implementation of body forces introduced in ref. 28 to incorporate the reaction term R_i. It is added to the right-hand side of (4):

$$R_i = t_i F_s \tag{25}$$

We can see easily that the following relation holds:

$$\sum_i R_i = F_s \tag{26}$$

A strong assumption is used here: we assume the reactions occur only locally, which means a local diffusive equilibrium which is always satisfied by the reaction.[7, 34]

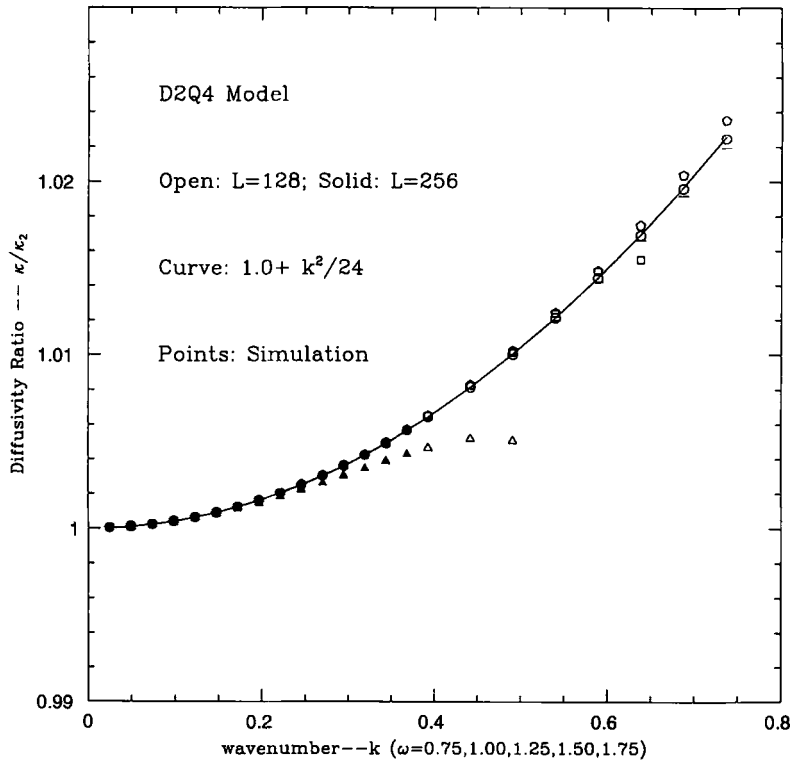

Fig. 2. Dispersion relation κ/κ_2 versus k. The open triangles, solid triangles, open squares, solid squares and open circles are numerical simulations corresponding to $\omega = 0.75$, 1.00, 1.25, 1.50, and 1.75, respectively. No critical value of ω_{cr} across which the κ_4 changes sign exists for the D2Q4 model.

4. SIMULATION RESULTS

We measure the diffusivity κ_2 as a function of the relaxation parameter ω in the purely diffusing case. The diffusivities of the D1Q2, D2Q4, and D3Q6 models differ only by a factor of the space dimension D. Good agreement between simulations and theoretical predictions is obtained (better than 0.1%). The dispersion relation has also been checked. Results are given in Figs. 1–3. The curves correspond to theoretical results κ/κ_2, while the points correspond to numerical simulations. Satisfactory agreement in all cases is achieved. The fourth-order corrections may have effects in the regime of large Knudsen number, i.e., large k and small ω. We see from these figures that the influence of ω on the dispersive behavior in the 1D case is opposite to the 3D case. In general, the fourth-order and higher

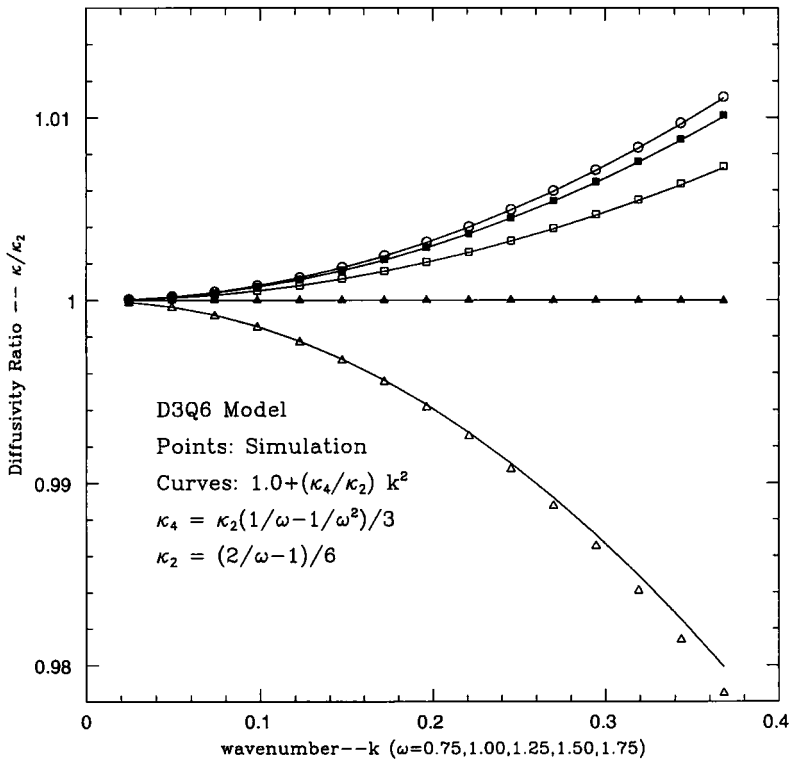

Fig. 3. Dispersion relation κ/κ_2 versus k for the D3Q6 model. The value of κ/κ_2 increases as ω increases for this model. The open triangles, solid triangles, open squares, solid squares, and open circles are numerical simulations corresponding to $\omega = 0.75$, 1.0, 1.25, 1.5, and 1.75, respectively. The critical value ω_{cr} is 1.0 for this model.

order terms can be neglected in the long wavelength (small k) and long-time limits (small Ω).

The front is a special kind of pattern, which has been extensively studied theoretically and experimentally.[26] On the one hand, there may exist some analytical solutions under certain conditions or some asymptotic behaviors can be studied; on the other hand, it is easier to prepare experimentally the two completely separated reacting components than to mix them up uniformly at the initial time without reactions. The irreversible $A + B \rightarrow C$ system looks "simple". However, no general analytical solution has been found[16] for general initial and boundary conditions. Figure 4 shows the density and production profiles at five different times for the case of equal density ratio, i.e., $\rho_{b0}/\rho_{r0} = 1$. Perfect symmetry is preserved. Figure 5 demonstrates the case with $\rho_{b0}/\rho_{r0} = 2$; in this case, we

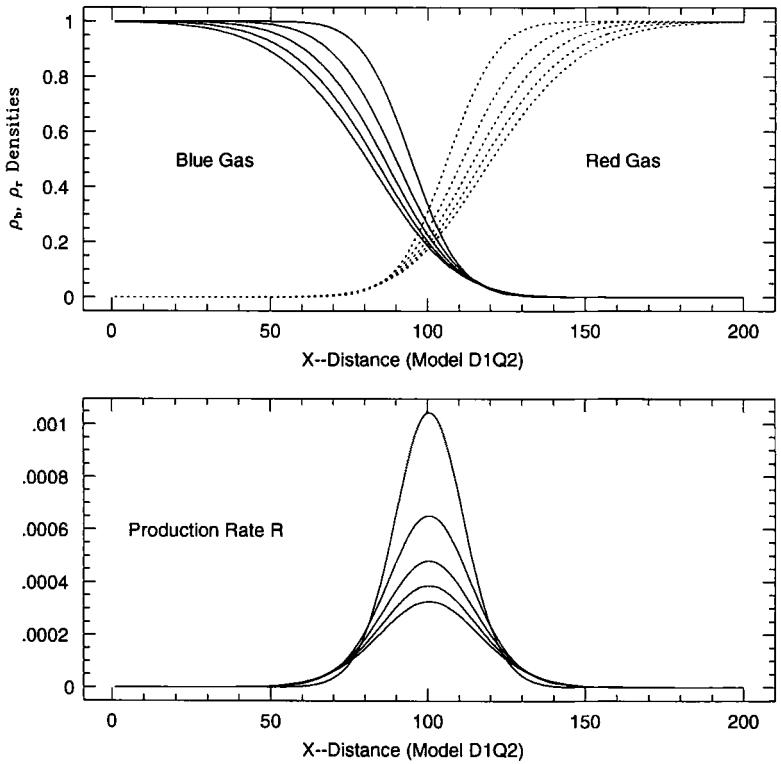

Fig. 4. Density profiles ρ_b and ρ_r (upper graph) and the production rate R (lower graph) for the D1Q2 model. Different curves correspond to different times: $T = 200$, 400, 600, 800, 1000. The parameters are $\rho_{b0} = \rho_{r0} = 1.0$, $\omega_b = \omega_r = 1.0$, and $K = 0.01$.

see the front moving to the right side. The scaling laws for this problem are shown in Figs. 6–8. They represent, respectively, the width of the front $W(T)$, the center of the front $x_f(T)$ for the asymmetric conditions, and the normalized production function $R(x, T) = K\rho_a\rho_b$. The width W is defined by

$$W^2(T) = \frac{\sum_{x=1}^{x=L} (x - x_f)^2 R(x, T)}{\sum_{x=1}^{x=L} R(x, T)} \sim T^{2\alpha} \tag{27}$$

the center x_f by

$$x_f(T) = \frac{\sum_{x=1}^{x=L} xR(x, T)}{\sum_{x=1}^{x=L} R(x, T)} \sim T^{1/2} \tag{28}$$

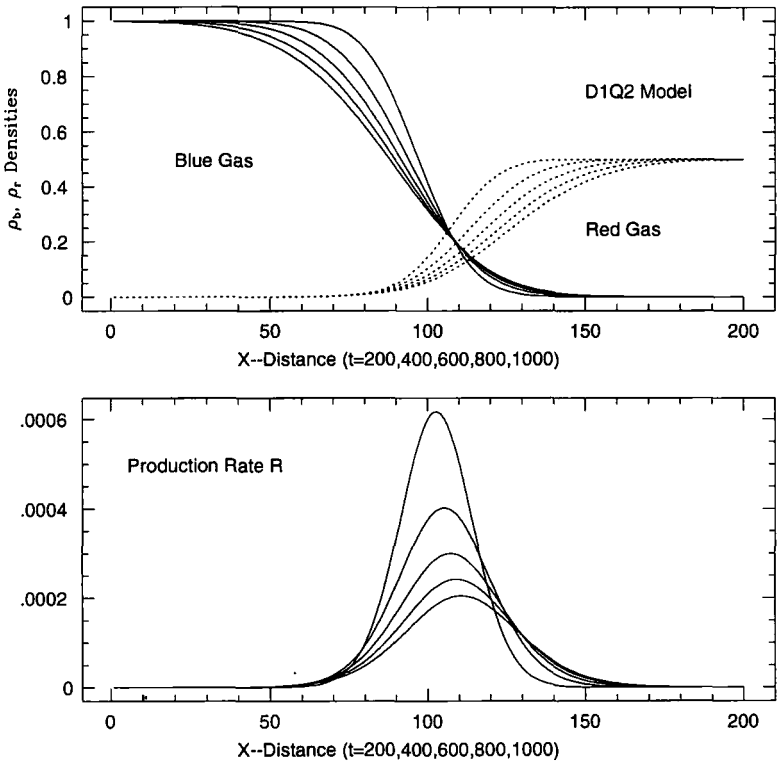

Fig. 5. Density profiles ρ_b and ρ_r (upper graph) and the production rate R (lower graph). Different curves correspond to different times: $T = 200$, 400, 600, 800, 1000. The parameters are $\rho_{b0} = 1.0$, $\rho_{r0} = 0.5$, $\omega_b = \omega_r = 1.0$, and $K = 0.01$.

and the production rate by

$$R(x, T) = K\rho_a\rho_b \sim T^{-\beta}G[(x - x_f)\,T^{-\alpha}] \tag{29}$$

Gálfi and Rácz[12] found that in the long-time regime $\alpha = 1/6$ and $\beta = 2/3$. From Figs. 6 and 8, we obtain the same exponents for long-time asymptotics. Figure 7 shows the 1/2 scaling for x_f. Figure 6 also shows a transitory regime between the long-time 1/6 scaling and a short-time 1/2 scaling which was not found in the asymptotic analysis. A scaling function is found from Fig. 8. We fit the curve with

$$G(\xi) \sim \exp\left(-\frac{\xi^2}{\sigma^2}\right), \qquad \sigma^2 = \frac{4\kappa_2}{3} \tag{30}$$

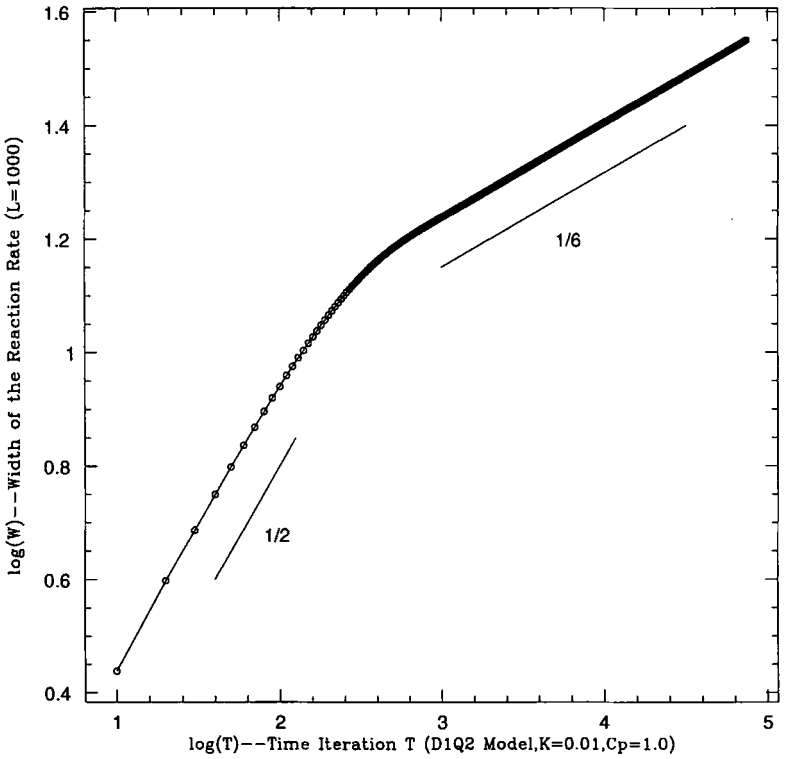

Fig. 6. Width of the front $W(T)$ as a function of time T; a log–log plot. The parameters are $\rho_{b0} = \rho_{r0} = 1.0$, $\omega_b = \omega_r = 1.0$, and $K = 0.01$. Two different regimes are clearly seen: the short-time 1/2 scaling regime and the long-time 1/6 asymptotics.

For different κ_2, the function agrees quite well with the numerical simulation for ξ near 0. A more detailed comparison with the results of Gálfi and Rácz is needed for large ξ since they found an Airy function behavior in that region.[12] An interesting problem to be studied is how scaling exponents depend on the space dimension and stochastic stirring processes. Our lattice BGK models without random stirring is a field description, therefore no space dimension dependence is expected. Local particle methods,[14] give a strong dependence of scaling exponents on space dimension. Bramson and Lebowitz[35] proved mathematically that $D=4$ is a critical value for the case of homogeneous, equal initial density distributions. The renormalization group (RG) approach was used to derive and to find new scaling exponents.[22] Therefore, it will be of interest to use

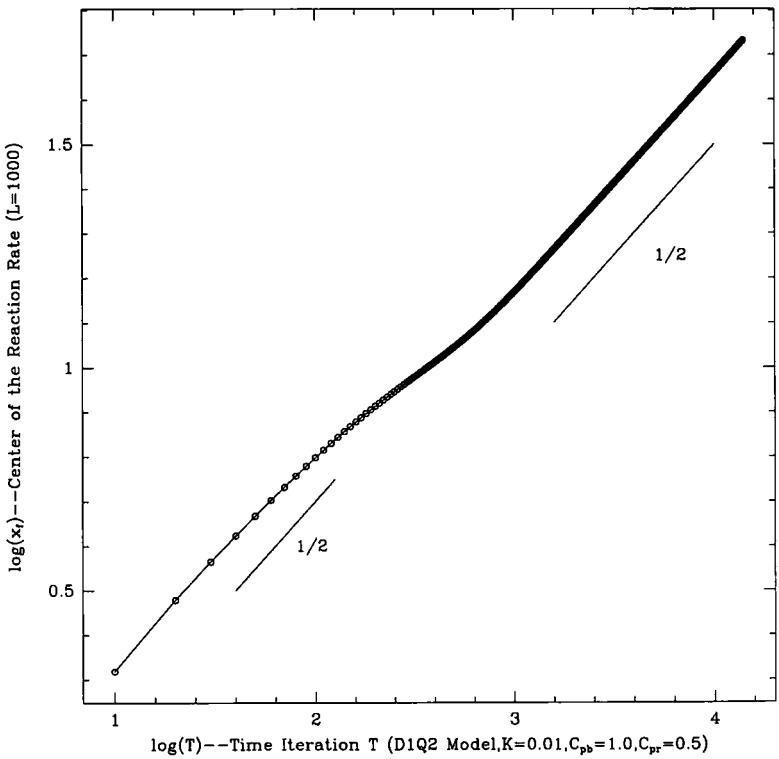

Fig. 7. Center of the front $X_f(T)$ versus time T, a log–log plot. The parameters are $\rho_{b0}=\rho_{r0}=1.0$, $\omega_b=1.0$, $\omega_r=0.5$, and $K=0.01$. A short transition exists between the short-time 1/2 regime and the long-time 1/2 asymptotics.

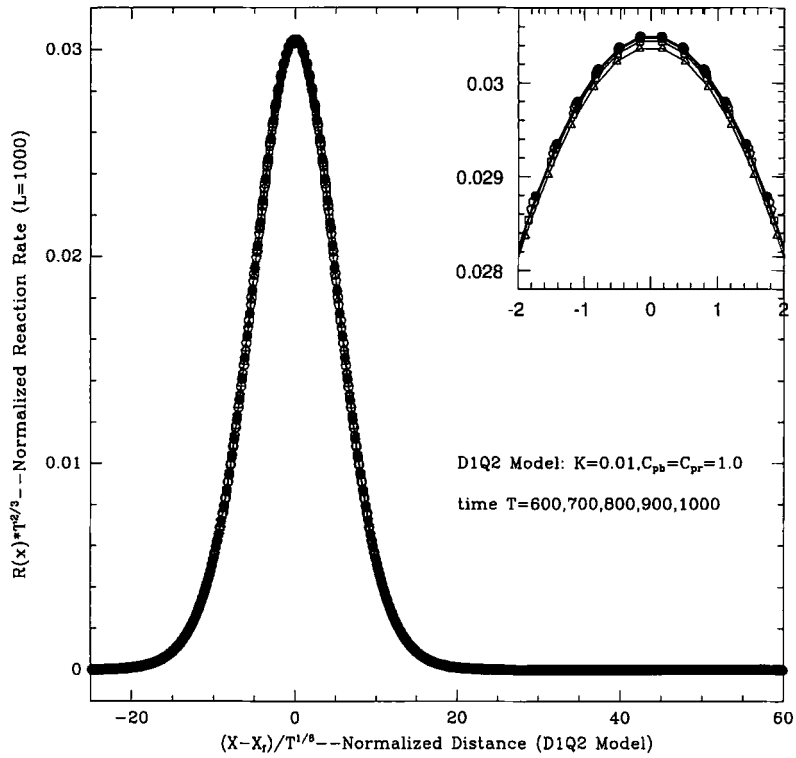

Fig. 8. Normalized rate $R(x, t) * T^{2/3}$ as a function of normalized distance $(X - X_f)/T^{1/6}$. Different symbols correspond to different times: triangles, square, pentagons, open circles, and solid circles are for time $T = 600$, 700, 800, 900, and 1000, respectively. The parameters are $\rho_{b0} = \rho_{r0} = 1.0$, $\omega_b = \omega_r = 1.0$, and $K = 0.01$. All data collapse on a single *Gaussian*-like scaling function.

noisy lattice BGK models to study coupling effects of space dimension and random stirring.

For the following chosen parameters of the Schlögl model,

$$F_R(\rho) = -K(\rho^3 - 1.5\rho^2 + 0.6875\rho - 0.09375), \qquad K = 0.01 \tag{31}$$

a bistable regime with $\rho_1 = 0.25$ and $\rho_2 = 0.75$ is predicted. Figure 9 shows the time evolution for the Schlögl model in two dimensions; a random initial density with mean density equal to 0.5 is used. Large-scale patterns are formed in the course of time; solid lines represent high densities (close to 0.75) and dashed lines low densities (close to 0.25). Figure 9 exhibits the capability of our model to capture such interesting behavior at large scale.

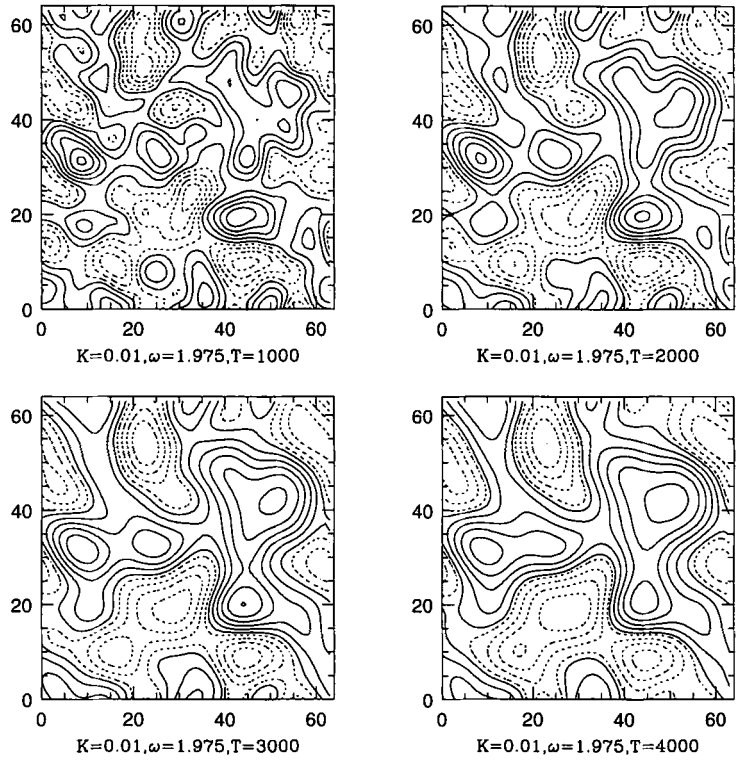

Fig. 9. Density contours at four times $T = 1000$, 2000, 3000, and 4000 for the Schlögl model in two dimensions. The solid lines represent high density; dotted lines represent lower density. The bistable regime is chosen as $F_R(\rho) = -K(\rho^3 - 1.5\rho^2 + 0.6875\rho - 0.09375)$.

More work about large-scale pattern formations (Turing structures) with detailed comparisons with experimental results and with numerical results of other numerical methods will be pursued.

5. CONCLUDING REMARKS

In this paper, the lattice BGK models have been used to study front dynamics and pattern formations in reaction–diffusion systems. As examples, the diffusion-driven reactive model ($A + B \rightarrow C$) and the Schlögl model have been tested. In the diffusion-driven case, we verified the asymptotic results concerning the scaling exponents α, β and the scaling function of the production rate G at long times. Noisy lattice BGK models may be introduced to study the dependence of space dimension and random stirring on scaling exponents. We have derived the fourth-order

corrections for the first time, and very accurate numerical results do confirm our theoretical predictions. The lattice BGK models use the mean-field approximation and are considered as a mesoscopic description of real systems. It provides a new numerical approach to understand complicated phenomena such as Turing structures.

ACKNOWLEDGMENTS

We would like to thank two referees for very helpful comments and for informing us of several useful references. This work was supported in part by AFOSR/DARPA contract F49620-91-C-0059 and by ONR/DARPA grant N00014-92-J-1796.

REFERENCES

1. R. Benzi, S. Succi, and M. Vergassola, *Phys. Rep.* **222**(3):145–197 (1992).
2. P. Bhatnagar, E. P. Gross, and M. K. Krook, *Phys. Rev.* **94**:511 (1954).
3. S. Chapman and T. G. Cowling, *The Mathematical Theory of Nonuniform Gases*, 3rd. ed. (Cambridge University Press, Cambridge, 1970).
4. H. D. Chen, S. Y. Chen, and W. Matthaeus, *Phys. Rev. A* **45**:R5339 (1992).
5. B. Chopard and M. Droz, *Europhys. Lett.* **15**(4):459 (1991).
6. D. Dab, J. P. Boon, and Y. X. Li, *Phys. Rev. Lett.* **66**(19):2535 (1991).
7. D. Dab, A. Lawniczak, J. P. Boon, and R. Kapral, *Phys. Rev. Lett.* **64**(20):2462 (1990).
8. D. d'Humières, P. Lallemand, and Y. H. Qian, *C.R. Acad. Sci. Paris* **308**:585 (1989).
9. G. D. Doolen, ed., *Lattice Gas Methods for Partial Differential Equations* (Addison-Wesley, Reading, Massachusetts, 1989).
10. U. Frisch, D. d'Humières, B. Hasslacher, P. Lallemand, Y. Pomeau, and J.-P. Rivet, *Complex Systems* **1**:649 (1987).
11. U. Frisch, B. Hasslacher, and Y. Pomeau, *Phys. Rev. Lett.* **56**:1505 (1986).
12. L. Gálfi and Z. Rácz, *Phys. Rev. A* **38**:3151 (1988).
13. R. Gatignol. *Théorie Cinétique des Gaz à répartition discrète de Vitesses* (Springer-Verlag, Berlin, 1975).
14. G. Giacomin, *Stoch. Proc. Appl.* **51**:25 (1994).
15. B. Hasslacher, R. Kapral, and A. Lawniczak, *Chaos* **3**(1):7 (1993).
16. S. Havlin, M. Araujo, H. Larralde, and H. E. Stanley, *Physica A* **191**:143 (1992).
17. F. J. Higuera and J. Jimenez, *Europhys. Lett.* **9**(7):663–668 (1989).
18. L. Kadanoff, G. McNamara, and G. Zanetti, *Complex Systems* **1**:791 (1987).
19. R. Kapral, A. Lawniczak, and P. Masiar, *Phys. Rev. Lett.* **66**(19):2539 (1991).
20. R. Kapral, A. Lawniczak, and P. Masiar, *J. Chem. Phys.* **96**(4):2762 (1992).
21. A. J. Koch and H. Meinhardt, *Rev. Mod. Phys.* **66**:1481 (1994).
22. B. P. Lee and J. Cardy, *Phys. Rev. E* **50**(5):R3287 (1994).
23. K. Maginu, *J. Math. Biosci.* **21**:17 (1975).
24. G. R. McNamara and G. Zanetti, *Phys. Rev. Lett.* **61**:2332 (1988).
25. J. D. Murray, *Mathematical Biology* (Springer, New York, 1989).
26. Conference on Models of Nonclassic Reaction Rates, *J. Stat. Phys.* **65** (1991).
27. S. Ponce Dawson, S. Y. Chen, and G. D. Doolen *J. Chem. Phys.* **98**(2):1514 (1993).

28. Y. H. Qian, Lattice gas and lattice kinetic theory applied to the Navier–Stokes equation, Ph.D. thesis, Ecole Normale Supérieure and University of Paris 6 (1990).
29. Y. H. Qian, unpublished (1990).
30. Y. H. Qian, D. d'Humières, and P. Lallemand, *Europhys. Lett.* **17**(6):479–484 (1992).
31. Y. H. Qian and S. A. Orszag, *Europhys. Lett.* **21**(3):255–259 (1993).
32. F. Schlögl, C. Escher, and R. S. Berry, *Phys. Rev. A* **27**:2698 (1983).
33. E. E. Sel'kov, *J. Biochem* **4**:79 (1968).
34. J. R. Weimar, D. Dab, J. P. Boon, and S. Succi, *Europhys. Lett.* **20**(7):627 (1993).
35. Bramson and Lebowitz, *J. Stat. Phys.* **62**(1/2):297 (1991).